A 4-DOF Exosuit Using a Hybrid EEG-Based Control Approach for Upper-Limb Rehabilitation

ZHICHUAN TANG[1,2]**, ZHIXUAN CUI**[1]**, HANG WANG**[1]**, PENGCHENG LIU**[3]**, (Member, IEEE),
XUAN XU**[1]**, AND KESHUAI YANG**[1]

[1]Industrial Design Institute, Zhejiang University of Technology, Hangzhou 310023, China
[2]Faculty of Science and Technology, Bournemouth University, BH12 5BB Poole, U.K.
[3]Department of Computer Science, University of York, YO10 5DD York, U.K.

CORRESPONDING AUTHOR: P. LIU (pengcheng.liu@york.ac.uk)

ABSTRACT Rehabilitation devices, such as traditional rigid exoskeletons or exosuits, have been widely used to rehabilitate upper limb function post-stroke. In this paper, we have developed an exosuit with four degrees of freedom to enable users to involve more joints in the rehabilitation process. Additionally, a hybrid electroencephalogram-based (EEG-based) control approach has been developed to promote active user engagement and provide more control commands. The hybrid EEG-based control approach includes steady-state visual evoked potential (SSVEP) paradigm and motor imagery (MI) paradigm. Firstly, the rehabilitation movement was selected by SSVEP paradigm, and the multivariate variational mode decomposition (MVMD) and canonical correlation analysis (CCA) method was used for SSVEP EEG recognition; then, the motion intention was obtained by MI paradigm, and the convolutional neural network (CNN) and long short-term memory network (LSTM) were used to build a CNN-LSTM model for MI EEG recognition; finally, the recognition results were translated into control commands of Bowden cables to achieve multi-degree-of-freedom rehabilitation. Experimental results show that the average classification accuracy of the CNN-LSTM model reaches to $90.07\% \pm 2.23\%$, and the overall accuracy of the hybrid EEG-based control approach reaches to $85.26\% \pm 1.95\%$. The twelve subjects involved in the usability assessment demonstrated an average system usability scale (SUS) score of 81.25 ± 5.82. Additionally, four participants who underwent a 35-day rehabilitation training demonstrated an average 10.33% increase in range of motion (ROM) across 4 joints, along with a 11.35% increase in the average electromyography (EMG) amplitude of the primary muscle involved. The exosuit demonstrates good accuracy in control, exhibits favorable usability, and shows certain efficacy in multi-joint rehabilitation. Our study has taken into account the neuroplastic principles, aiming to achieve active user engagement while introducing additional degrees of freedom, offering novel ideas and methods for potential brain-computer interface (BCI)-based rehabilitation strategies and hardware development. Clinical impact: Our study presents an exosuit with four degrees of freedom for stroke rehabilitation, enabling multi-joint movement and improved motor recovery. The hybrid EEG-based control approach enhances active user engagement, offering a promising strategy for more effective and user-driven rehabilitation, potentially improving clinical outcomes. Clinical and Translational Impact Statement: By developing an exosuit and a hybrid EEG-based control approach, this study enhances stroke rehabilitation through better user engagement and multi-joint capabilities. These innovations consider neuroplasticity principles, integrating rehabilitation theory with rehabilitation device.

INDEX TERMS Exosuit, Bowden cable, motor imagery, SSVEP, rehabilitation.

I. INTRODUCTION

ALTHOUGH stroke mortality is decreasing, the prevalence of individuals living with the effects of stroke has increased due to the expanding and aging population [1]. Under the trend of aging, it is increasingly difficult for traditional rehabilitation methods to cope with the surging demand

for rehabilitation. In contrast to labor-intensive techniques like manual therapy or therapist-assisted exercises, rehabilitation exoskeletons provide consistent support throughout the rehabilitation process, ensuring stable and continuous assistance. By leveraging high-precision sensors and biomedical signals, such as inertial measurement units (IMU), electromyography (EMG) signals, and electroencephalogram (EEG) signals, good control performance and tracking and evaluation of rehabilitation effect can be achieved [2], [3]. Traditional exoskeletons which typically use rigid frames to apply driving torque to joints, present a number of challenges for rehabilitation, such as high weight and large structural size [4]. In contrast to rigid exoskeletons, soft exoskeletons have demonstrated superior performance in terms of portability, safety and weight [5], [6]. The compliant and light structure eliminates joint misalignment issues and does not restrict the user's independent movement. And it can also be easily worn, replacing some rigid exoskeletons that performed rehabilitation tasks in a fixed posture.

In work related to exosuits, the chosen actuation method determines the main hardware characteristics of the exosuit, further influencing its weight and level of portability. Nam et al. [7] developed an innovative EMG-driven exoneuromusculoskeleton designed for self-help upper limb training following stroke. The soft pneumatic muscle helped achieve the structural characteristics of lightweight and compact design, but this structure still required most of the hardware to be fixed to the surface of the arm. On the contrary, Bowden cables consist of inner wires and outer casings, enabling force transmission while providing flexibility and compliance. They extend the distance between the actuated joint and the actuator, facilitating remote actuation. Wu et al. [8] developed a tendon-sheath actuator unit and optimized the control strategy to achieve stable elbow joint movement. They integrated most of the hardware on the user's back, resulting in a more portable design. Nycz et al. [9] aimed for lightweight design and placed the actuation module and electronics module on the upper back. Similarly, they achieved excellent weight performance through remote actuation with Bowden cables. In practical development, both exosuits and Bowden cables exhibit multiple advantages, particularly in achieving lightweight design and enabling unrestricted user mobility [10]. However, there is still considerable room for improvement in terms of the size of the hardware structure, the layout of the actuation module, the number of degrees of freedom and weight.

Some rehabilitation exoskeletons are designed to perform pre-set repetitive movements, with patients engaging in a passive role [11], [12]. This method, similar to continuous passive motion (CPM), can sometimes limit rehabilitation effectiveness [13]. To overcome this, researchers have developed various exoskeletons that aim to boost user engagement and improve rehabilitation outcomes [14], [15]. Recent studies show that neuroplasticity plays a key role in recovery after nerve injury. Patients who actively participate in their

rehabilitation are better able to promote neuroplasticity [16]. Translating these findings into clinical practice involves designing rehabilitation exoskeletons that incorporate task-specific exercises, high-repetition movements, and personalized therapy regimens, all of which are crucial for promoting neuroplasticity [17]. Huang et al. [18] have developed a hand rehabilitation system, emphasizing the importance of neuroplasticity, especially with high-repetition training. The clinical measurements show a 35% average improvement in training effectiveness. Compared to biomechanics-based or passive rehabilitation, incorporating neuroplastic principles and promoting user engagement is a positive and beneficial exploration for rehabilitation outcomes. However, the effectiveness of such approaches still requires further intricate work for validation. For the evaluation of exosuits intended for rehabilitation purposes, it is often a complex task that frequently encounters issues such as individual differences, consistency of procedures, and participant dropouts midway through the process. In the work of Proietti et al., they developed a soft inflatable robotic glove for stroke survivors to use independently at home. After 4 weeks of use by ten chronic moderate-to-severe stroke survivors, significant improvements were observed in Fugl-Meyer Assessment (FMA) scores and range of motion (ROM), demonstrating the effectiveness of remote and autonomous rehabilitation [19].

Brain-computer interface (BCI) can convert EEG signals from brain activity to output commands [20]. Among various BCI paradigms, motor imagery (MI) and steady-state visual evoked potential (SSVEP) are widely used for their high performance [21], [22]. SSVEP is widely used because of its high accuracy and stability, less training required, and lower subject differences [23], [24]. It can offer numerous control commands, typically distinguishing several to tens of commands [25]. Research by Bakardjian et al. indicates that flashing stimuli at frequencies from 5.6 to 15.3 Hz, peaking at 12 Hz, elicit the strongest response, with weaker responses at 28 and 42 Hz. In an eight-command BCI system, the average accuracy was 98% with a 3.4-second delay [26]. Multivariate variational mode decomposition (MVMD) extends variational mode decomposition (VMD) to multi-channel signals [27]. MVMD can decompose multi-channel SSVEP EEG signals into several multivariate modulated oscillations, effectively leveraging the different characteristics of the harmonic spectrum. As a result, MVMD has the potential to enhance the canonical correlation analysis (CCA) algorithm and its application in BCI control [28]. MI is notable for its independence from physical movement, naturally promoting brain activity [29]. When users imagine their own body movements, the primary motor cortex of the brain exhibits desynchronization of neural activity, called event-related desynchronization (ERD) or synchronization (ERS). Specifically, μ waves (8-14 Hz) and β waves (14-30 Hz) are the main frequency spectra of ERS and ERD [30]. Generally, MI paradigm can provide two relatively stable control commands. Introducing more commands would result in a

significant decrease in accuracy and user fatigue [31]. As our study aims to develop an exosuit with four degrees of freedom, using MI alone may not generate a sufficient number of control commands. Therefore, we have developed a hybrid EEG-based control approach that combines SSVEP and MI paradigms to provide more control commands and realize active rehabilitation.

Controlling an exosuit with EEG signals is a complex task that involves overcoming the challenge posed by the low signal-to-noise ratio of EEG signals. In recent years, in addition to traditional EEG feature extraction and classification methods, deep learning algorithms such as convolutional neural network (CNN) have also been applied to MI classification. Tabar et al. [32] used CNN and stacked autoencoders (SAE) for feature extraction and classification of MI EEG signals, and achieved better classification performance by improving the input form, with a 9% increase compared to the winner algorithm of BCI IV 2b. Sakhavi et al. [33] used a new temporal representation of the data and a CNN architecture for classification. This new representation was achieved by modifying filter bank common spatial patterns (FBCSP), and the final framework improved by 7% compared to the winner algorithm of BCI IV 2a. However, EEG signals are fundamentally unstable time series signals. Therefore, combining time series information can also improve the classification accuracy of EEG [34], [35]. Meanwhile, long short-term memory network (LSTM) has been widely used in the processing of EEG signals. LSTM solves the problem of recurrent neural network (RNN) gradient disappearance by introducing gate mechanisms. In the work of Schirrmeister et al., 44 channels of EEG data went through temporal convolution with 25 linear filters, and spectral features were used to extract and characterize specific frequency components of the EEG signals [36]. Wang et al. [37] proposed a LSTM-based network for classifying MI tasks, which achieved excellent performance by extracting effective features through a one dimensional-aggregation approximation. LSTM can better capture the dependencies between time-series data, thus improving the performance of classification.

In this paper, we aim to integrate a lightweight four-degree-of-freedom exosuit with an active control approach to enhance rehabilitation outcomes, distinguishing it from the commonly observed single-joint or two-joint assistive exoskeletons in related studies. The exosuit is actuated by Bowden cables, which are characterized by their lightweight, compact size, and remote actuation capabilities. This design allows us to achieve four degrees of freedom in rehabilitation with a straightforward hardware structure. In terms of control, we propose a hybrid EEG-based control approach that combines SSVEP and MI paradigms to provide more control commands, enhance user engagement, and improve rehabilitation outcomes. For SSVEP paradigm, we use the MVMD-CCA algorithm. The application of MVMD-CCA improves the detection ability of SSVEP EEG signals, enabling accurate and fast classification. Meanwhile, we

developed a CNN-LSTM model to improve the classification performance of MI EEG signals. We conducted both offline and online experiments and compared them with existing algorithms. Finally, we conducted both usability assessment and rehabilitation assessment. Usability assessment was performed using the system usability scale (SUS) to assess users' experience and ease of use with the exosuit. The rehabilitation assessment involved capturing changes in participants' average EMG amplitudes and joint ROM across multiple joints after 35 days of rehabilitation training. These changes were used to validate the multi-joint rehabilitation effects.

II. EXOSUIT DESIGN
A. DESIGN GOALS
The exosuit we developed facilitates rehabilitation in the upper limbs for four joints: non-thumb fingers, wrist, elbow and shoulder. The following features of exosuit should be implemented while ensuring the actuating effect.

1) ACTIVE CONTROL
Active control performance enables users to perform rehabilitation more actively and independently, improving their level of participation and confidence, as well as rehabilitation outcomes. And it directly affects operability and usability of the exosuit.

2) MULTIPLE DEGREES OF FREEDOM
Multi-degree-of-freedom control can better simulate the movements of human muscle and skeletal system, providing more natural and smooth rehabilitation tasks. In addition, utilizing the features of Bowden cables, we can transmit power with a small volume and lightweight structure, which enables us to replicate our method on multiple joints, achieving coordinated control with multiple degrees of freedom.

3) COMFORTABLE, PORTABLE, AND LOW-COST
Good usability and portability allowing users to easily use it without the help of others and adapt to possible home-use conditions. Low cost is also essential, which can ensure better production and promotion of the exosuit. At the same time, the exosuit should be as light and comfortable as clothing to reduce the burden of using.

B. HARDWARE DESIGN AND MATERIALS
Fig. 1 shows the structure of the exosuit. We use nylon shirt fabric as the basic carrier, and the exosuit is comprised of three parts: strap module, Bowden cable actuation module and electronics module. Strap module enables the exosuit to closely conform to the user and provide some room for size adjustments to accommodate individual differences. Unlike rigid exoskeletons that can apply power directly to the joints, the exosuit can only avoid deformation of the flexible part by closely fitting the actuated joint, thus allowing the Bowden cables to exert power more effectively on the joint. The strap module is also used as a carrier to fix other structures, such as

FIGURE 1. Hardware structure.

inner wires, outer casings and end connectors, which are all fixed on the surface of the strap module. The inner wire and outer casing are crucial parts of the Bowden cable actuation module, extending and fixed along the direction of muscle action on the strap module. The other components of the Bowden cable actuation module are placed in a 3D-printed box, including actuators, screw rods, and 3D-printed limit rods. The electronics module integrates a CNC Shield V3 board, an Arduino Uno board, a 2800 mAh battery, and other interfaces, which are also set in a 3D-printed box and placed under the actuation module box.

1) 4-DOF BOWDEN CABLE ACTUATION MODULE
Compared with other actuation methods, Bowden cables are small in size and light in weight, and can easily pass through narrow and tortuous spaces while providing power transmission. By referencing the position and direction of the muscles, we can set the position of the Bowden cable to determine the location and angle of the actuation. The exosuit we developed actuates four joints, including finger flexion, wrist flexion, elbow flexion, and shoulder internal rotation. The specific structure of Bowden cable actuation module is shown in Fig. 2.

In real life, most movements rely on the coordinated work of multiple joints. For example, grabbing desk items requires the cooperation of shoulder joints, elbow joints, and finger joints, while moving objects and drinking water require the involvement of wrist joints. Due to the complexity of the musculoskeletal system, it is very challenging to develop an exosuit that can perform multiple complete movements. Currently, many exosuits are designed to primarily assist specific joints, including the elbow, wrist, and finger joints. Most of these exosuits typically support only 1-2 joints. However, in the case of the elderly, their shoulder joint tends to experience a more rapid loss of strength compared to the other three
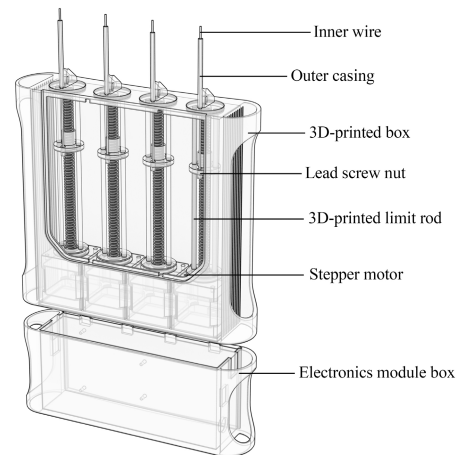
FIGURE 2. Structure of Bowden cable actuation module.

joints [38]. In Gaponov's cable-driven exosuit, the method for actuating the shoulder joint is demonstrated by extending the suspended fulcrum above the shoulder to increase the length of the lever arm, generating sufficient power to assist shoulder abduction. However, this sacrifices the stability of the exosuit and makes the structure much more complex [39]. This reflects the current limitations in the development process of exosuits, as it is often challenging to balance the actuating of the shoulder joints with the portability of the exosuit. So we have abandoned external rotation of the shoulder joint and opted to support only the internal rotation of the shoulder joint to ensure a simpler structure for the exosuit. Specifically, the anchor point is set on the inner side of the right upper arm, and the actuating direction is from right to left. The Bowden cable passes front side of the nylon shirt, and this layout poses a challenge to portability of wearing. Thus, we assembled a 3D-printed quick-release connector at the end of the inner
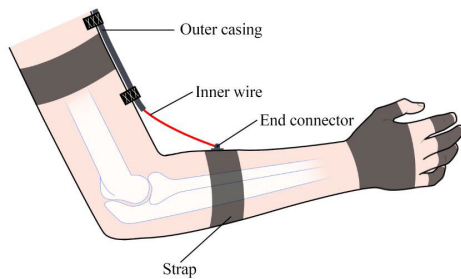
FIGURE 3. Bowden cable structure for actuating the elbow joint.

wire, which users can fix on the inner upper arm anchor point after wearing the exosuit.

Bowden cables consist of an outer casing and an inner wire. The outer casing serves mainly to protect and guide the inner wire, preventing interference from external friction and ensuring dynamic efficiency. As shown in Fig. 3, outer casings are fixed on the surface of the strap module along the direction of muscle extension, forming a channel for power transmission. The end of the outer casing extends the inner wire, and the end of the inner wire is fixed to the anchor point on the surface of the joint being pulled. The direction of the power is towards the end of the outer casing. Fig. 3 shows how the inner wire pulls the elbow joint into flexion.

2) WEIGHT OPTIMIZATION

The weight of the exosuit can directly affect the user's wearing burden. During the prototype development process, we took into account the weight performance of each module. This required us to balance weight and power when selecting the actuator. The driving distance and power requirement also dictated a certain motor specification to achieve the design goals. We selected a stepper motor with a 125mm length screw, with a single maximum driving force of 65N and a weight of 230g. We chose inner wire and outer casing products from Shimano (Shimano Ultimate, 5mm, Sakai, Osaka, Japan), which are excellent in weight and friction. For the battery, we selected a 2800 mAh lithium battery. With a lightweight design approach for each module, we achieved a weight of 2374 grams for the exosuit.

C. CONTROL STRATEGY

SSVEP, as an external stimulus, presents challenges in promoting the motivation of subjects. In addition, MI paradigm poses challenges in providing sufficient number of commands. Therefore, we combined the advantages of both to provide more control commands and to realize active rehabilitation. The SSVEP and MI paradigms are used for the respective purposes of selecting rehabilitation movements and recognizing motor intentions.

1) HYBRID EEG-BASED CONTROL APPROACH

The hybrid EEG-based control approach is shown in Fig. 4, which includes two steps: a selection step and a recognition

step. We define these two steps as STEP1 and STEP2 respectively. In STEP1, we ran a pre-designed flashing stimuli program on the computer screen. The stimulus program contains 7 images representing 7 different rehabilitation movements, evenly distributed on the computer screen, flashing at frequencies ranging from 10 to 16Hz. The 7 images and their corresponding flashing frequencies are shown in Fig. 5. These movements encompass four single-joint movements and three multi-joint coordinated movements, involving the finger, wrist, arm, elbow, moving a cup, lifting a dumbbell, and drinking. After starting the program, subjects visually select one of the seven predetermined movements by directing their gaze towards it. We collect SSVEP signals from eight electrodes located in the occipital lobe, including POz, PO3, PO4, PO5, PO6, Oz, O1, and O2, to obtain eight-channel SSVEP signals.
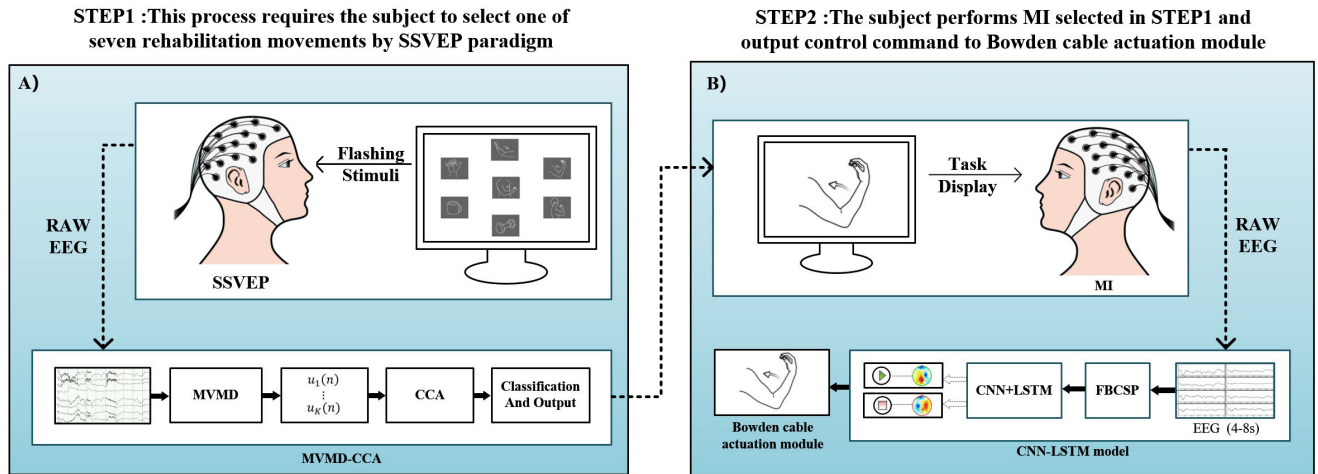
MVMD and CCA were used for SSVEP EEG recognition. CCA and its improved algorithms have been widely used for the recognition of SSVEP in BCI, demonstrating excellent performance in terms of speed and accuracy [40], [41]. Considering the advantages of multivariate modulated oscillations and the multichannel nature of EEG signals, we employ an MVMD-CCA algorithm [27] to enhance the recognition accuracy of SSVEP.

In the hybrid EEG-based control approach, STEP2 is focused on identifying right-hand MI to trigger the exosuit's movement. This binary classification distinguishes right-hand MI (positive class) from all other states, including resting and left-hand MI, which are grouped as 'non-right-hand MI' (negative class). During the STEP2, the subject is required to perform MI to output control commands. When the subject performs right-hand MI, the recorded EEG signal will be filtered by the FBCSP method and then undergoes feature extraction and classification by the CNN-LSTM model we built. If the classification result is right-hand MI, we can infer that the subject is in an active participation state in the selected movement, and the control command will be sent to the Bowden cable actuation module to actuate the movement selected in STEP1. In this process, CNN-LSTM model is used to decode the spatial and temporal features in the MI signal, and the proposed method can achieve satisfactory results in subsequent experiments. Fig. 6 shows the complete process of the hybrid EEG-based control approach.

2) ALGORITHM

In STEP1, the subject selects a movement by gazing at images flashing at different frequencies. The collected EEG signals are preprocessed to enhance quality through filtering and artifact removal. The CCA algorithm calculates the correlation between the EEG signals and reference signals generated by visual stimuli at different frequencies.

We define f_i as the target stimulus frequency and Y_i as the reference matrix containing the fundamental wave and harmonics, which generate the SSVEP response. The reference

STEP1 : This process requires the subject to select one of seven rehabilitation movements by SSVEP paradigm

STEP2 : The subject performs MI selected in STEP1 and output control command to Bowden cable actuation module

FIGURE 4. Hybrid EEG-based control approach. (A) Selection step. The selection step uses the SSVEP paradigm to allow the subject to choose 1 of 7 movements. The result classified by MVMD-CCA will be sent to STEP2; (B) Recognition step. The movement selected in STEP1 is played on the computer screen, and the subject performs MI, and then the collected EEG data will be sent to the CNN-LSTM model for classification, and then sent control command to the Bowden cable actuation module.
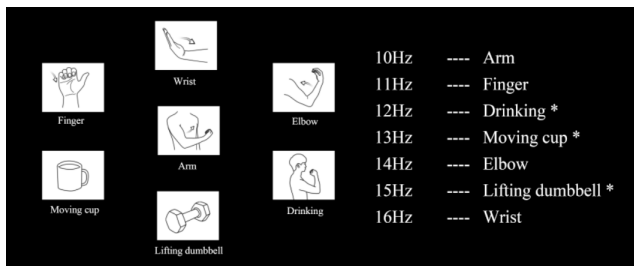
FIGURE 5. The corresponding relationship between the movement and its flashing frequency, the movement marked with an asterisk means that the movement is a multi-joint movement.

matrix is expressed as follows:

$$Y_i = \begin{pmatrix} \sin(2\pi f_i n) \\ \cos(2\pi f_i n) \\ \vdots \\ \sin(2\pi N_h f_i n) \\ \cos(2\pi N_h f_i n) \end{pmatrix}, \tag{1}$$

$$n = \frac{1}{f_s}, \frac{2}{f_s}, \dots, \frac{M}{f_s}, \tag{2}$$

where N_h represents the harmonic order, f_s represents the sampling frequency, and M represents the number of sampling points. For j multi-channel SSVEP signals $X = (x_1, x_2, \dots, x_j)^T$, the correlation coefficient ρ between X and each stimulation frequency reference matrix Y_i calculated by CCA is shown in the following equation.

$$\rho = \max_{W_X, W_Y}$$

$$= \frac{E[W_X^T XY^T W_Y]}{\sqrt{E[W_X^T XX^T W_X] E[W_Y^T YY^T W_Y]}}$$

$$= \frac{W_X^T C_X Y W_Y}{\sqrt{W_X^T C_X X W_X W_Y^T C_Y Y W_Y}} \tag{3}$$

The CCA algorithm seeks to find optimal linear transformations W_X and W_Y to maximize the correlation coefficient ρ_i between the SSVEP signal X and each reference matrix Y_i. Each obtained correlation coefficient is used as a feature dimension, resulting in a seven-dimensional feature vector $[\rho_1, \rho_2, \rho_3, \rho_4, \rho_5, \rho_6, \rho_7]$ for the seven stimulus targets.

The MVMD-CCA algorithm is proposed to enhance the detection performance of the CCA algorithm for SSVEP. MVMD reconstructs the input signal with minimal bandwidth. Using the Hilbert transform for modeling, MVMD decomposes the input data $x(n) = [x_1(n), x_2(n), \dots, x_C(n)]$ into K multivariate oscillations, as follows:

$$x(n) = \sum_{k=1}^{K} u_k(n), \tag{4}$$

where $u_k(n) = [u_{k,1}(n), u_{k,2}(n), \dots, u_{k,C}(n)]$ is the kth multivariate oscillation obtained by MVMD. The analytic signal $u_k^+(n)$ of $u_k(n)$ can be obtained using the Hilbert transform

$$u_+^k(n) = \begin{pmatrix} \left(\delta(n) + \frac{j}{\pi n}\right) u_{k,1}(n) \\ \left(\delta(n) + \frac{j}{\pi n}\right) u_{k,2}(n) \\ \vdots \\ \left(\delta(n) + \frac{j}{\pi n}\right) u_{k,C}(n) \end{pmatrix}. \tag{5}$$

By introducing MVMD, multichannel EEG signals are processed more effectively, which enhances classification accuracy. Meanwhile, the CCA algorithm directly performs classification by comparing the values of correlation coefficient, resulting in fast classification speed. If the correlation coefficient ρ_i is below a set threshold θ, it is considered
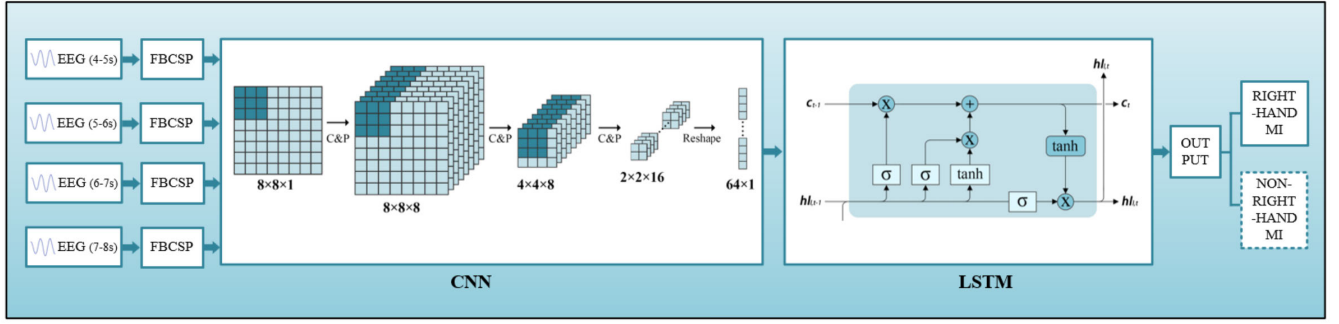
FIGURE 6. The specific structure of CNN-LSTM model. "C&P" represents convolution and pooling, "S" represents the sigmoid activation function, "tanh" represents the hyperbolic tangent activation function, "+" denotes plus, and "×" represents multiplication. The "C_t" indicates the state of the LSTM cell at the current moment.

that the subject's state is inactive or the signal quality is insufficient to ensure the accuracy of the classification results, and thus the current round of classification is skipped. For more details on the MVMD algorithm, refer to [27] and [42].

In STEP2, we used CNN-LSTM model, which consists of three stages: FBCSP, CNN and LSTM. As shown in Fig. 6, we segmented the 4-second MI EEG signal into 4 windows, each with a length of 1 second. Then, for each window, we process the signal using FBCSP and CNN respectively to obtain the spatial features of the EEG signal. Next, the spatial features obtained from each window are used as time-series inputs to the LSTM to extract the temporal features and perform classification of the signal. The final output of the model is the classification result of right-hand MI or non-right-hand MI.

CSP is a classic algorithm that can be used for signal recognition and analysis in the Event-Related Desynchronization/Event-Related Synchronization (ERD/ERS). FBCSP is an extended version of CSP, which adds more filters to extract EEG signal features at different frequencies. In the FBCSP algorithm we use, the Chebyshev type II filter is used to decompose the EEG of 4 windows into 8 frequency bands, including the frequency of 8-26 Hz, each filter bandwidth is 4 Hz with a 2 Hz overlap, and the center frequencies of the filters are 10 Hz, 12 Hz, 14 Hz, 16 Hz, 18 Hz, 20 Hz, 22 Hz, and 24 Hz, respectively. Where $Z_{b,t}$ represents the feature of FBCSP, X_b^T is the EEG signal of the bth bandpass filter in the tth (1-4) time window, $W_{b,j}^T = [W_{b,1}^T, W_{b,2}^T, W_{b,3}^T, W_{b,4}^T]$ represents the weights of the FBCSP filter. The matrix $C_{b,j}$ is the covariance matrix of the bth bandpass filter signal for the jth class of MI signal, and $E_{b,j}$ is the diagonal matrix containing the eigenvalues of $C_{b,j}$.

$$Z_{b,t} = W_b^T X_{b,t},$$
$$C_{b,j} W_{b,j} = \left(\sum_{j=1}^4 C_{b,j} \right) W_{b,j} E_{b,j}, \qquad (6)$$

for each class, we select the CSP features for the EEG signals of the tth time window of the tth bandpass filter. The CSP

feature is expressed as

$$f_{b,t} = \log \frac{\text{diag}(\hat{W}_b^T X_{b,t} X_{b,t}^T \hat{W}_b)}{\text{tr}(\hat{W}_b^T X_{b,t} X_{b,t}^T \hat{W}_b)}, \qquad (7)$$

where $\hat{W}_b$ represents the combining matrix of the first 2 and last 2 columns of $W_{b,j}$ ($j = 1, 2, 3, 4$), diag(·) denotes the diagonal elements of a matrix, tr(·) denotes the trace of a matrix, $f_{b,t}$ is the output of FBCSP in the form of feature vectors which are input into the CNN model. The size of the feature vector is 8×8, and the CNN model incorporates 2 hidden layers as shown in Fig. 6. In each convolutional layer, the input signal is convolved with a 3×3 filter kernel, and the activation function R is used to transform linear operations into non-linear ones. The output of each convolutional layer is expressed as

$$hc_l = R(\text{conv}(W_l, x_l) + b_l), \qquad (8)$$

where conv represents the convolution operator, x_l is the input of the l-th hidden layer, W_l is the weight matrix, b_l is the bias value, and hc_l is the output of the l hidden layer. The activation function R is chosen as the rectified linear unit (RELU) function. The RELU function is defined as

$$\text{RELU}(a) = \max(0, a). \qquad (9)$$

After two convolutional layers, a 2×2 max pooling layer is used to reduce the size of the feature matrix. Through the CNN, we obtain hc_3 with a size of $2 \times 2 \times 16$, which is then reshaped to a 1×64 output, denoted as o_t, to fit the input shape of the LSTM. Here, t represents the t-th time window. The CNN structure is shown in Fig. 6.

The input signal to the LSTM is defined as $x_{1,t} = o_t$, ($t = 1, 2, 3, 4$). The main feature of the LSTM contains three gates: the forget gate, external input gate, and output gate. The forget gate decides what information to discard from the previous unit and can be expressed as

$$f_{l,t} = \sigma(W_l^f \cdot [h_{l,t-1}, x_{l,t}] + b_l^f), \qquad (10)$$

where $h_{l,t-1}$ represents the output of the prior cell, $x_{l,t}$ is the input to the hidden layer, l represents the lth hidden layer, W_l^f

and b_l^f present the weight matrix and bias value, and σ is the sigmoid function that determines the degree of forgetting of information.

The structure of the external input gate is similar to that of the forget gate, and is specifically designed to learn new knowledge to replace forgotten information,

$$i_t = \sigma(W_l^i \cdot [h_{l,t-1}, x_{l,t}] + b_l^i), \qquad (11)$$

$$\hat{C}_t = \tanh(W_l^c \cdot [h_{l,t-1}, x_{l,t}] + b_l^c), \qquad (12)$$

where W_l^i, W_l^c, b_l^i and b_l^c are the weight matrix and bias values, respectively. The LSTM unit $C_{l,t}$ can be updated by the following equation.

$$C_{l,t} = f_{l,t} \cdot C_{l,t-1} + i_{l,t} \cdot \hat{C}_{l,t}. \qquad (13)$$

Finally, we obtain the output $h_{l,t}$ by the output gate. The output vector y of the entire neural network is equal to the output of the LSTM, which is $h_{3,4}$.

$$o_{l,t} = \sigma(W_l^o \cdot [h_{l,t-1}, x_{l,t}] + b_l^o), \qquad (14)$$

$$h_{l,t} = o_{l,t} \cdot \tanh(C_{l,t}). \qquad (15)$$

III. EXPERIMENTS

To evaluate the performance of the hybrid EEG-based control approach and the exosuit in real-world environment, we designed both an offline training experiment and an online control experiment. In the offline training experiment, we developed a CNN-LSTM model for each subject in the experiment to classify the user's motion intention in STEP2. In the online control experiment, the subjects used our exosuit, and we evaluated its performance in the rehabilitation tasks. In addition, we conducted usability assessment and rehabilitation assessment. Usability assessment utilized the SUS to access users' experience and ease of use of the exosuit. The rehabilitation assessment aimed to validate and evaluate the effectiveness of the exosuit in multi-joint rehabilitation under long-term usage conditions.

Nine healthy graduate students (6 males and 3 females, age:24 ± 2, height:169 ± 9 cm, weight:60 ± 12 kg) and three moderate stroke survivors (1 male and 2 females, age:62 ± 3, height: 162 ± 5 cm, weight:56 ± 9 kg) participated in our offline experiment, online experiment and usability assessment. Additionally, four stroke survivors (2 males and 2 females, age:64 ± 4, height:165 ± 7 cm, weight:56 ± 8 kg) with muscle weakness participated in our rehabilitation assessment. Each subject signed informed consent forms before the experiment, and the experiment was reviewed and approved by the Ethics Committee of the Zhejiang University of Technology.

A. OFFLINE TRAINING EXPERIMENT

The aim of the offline training experiment was to obtain the CNN-LSTM model for each subject. Subjects wore an EEG cap connected to the Biosemi acquisition device (ActiveTwo, BioSemi instrumentation, the Netherlands) to collect 28-channel data (FC5, FC3, FC1, FCz, FC2, FC4, FC6, C5, C3,
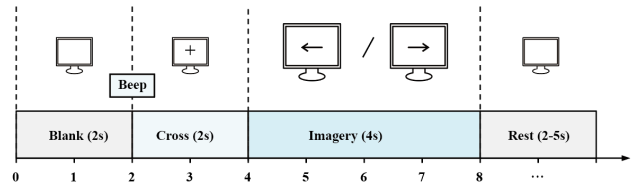

FIGURE 7. Timing diagram of one trial.

C1, Cz, C2, C4, C6, CP5, CP3, CP1, CPz, CP2, CP4, CP6, P5, P3, P1, Pz, P2, P4, P6). The reference electrode was placed at the mastoid of the left ear, and the ground electrode consisted of two independent electrodes, CMS and DRL. Conductive gel was used to reduce the impedance between the electrodes and the scalp to ensure that the impedance value of each electrode was below 5 kΩ. The sampling rate of the device was 1000 Hz.

The experiment required subjects to sit in front of a computer screen with their hands naturally resting on the desk in a relaxed state. They were asked to avoid blinking their eyes and making unnecessary head or body movements as much as possible. Fig. 7 shows the timing diagram of one trial. Each subject was required to complete 240 trials, including 120 left-hand MI and 120 right-hand MI. Each trial lasted for 8 seconds, starting with an acoustical warning tone at second 2 and a 2-s "+" sign presentation. Then, a cue ("←" or "→") randomly appeared on the screen (seconds 4-8) to indicate the left hand or right hand movement that the subject needed to imagine. To avoid fatigue, there was a random interval of 2-5 seconds between each trial and a 2-minute rest period between every 30 trials. The 4-second MI EEG (seconds 4-8) of each trial was used as an input sample for the hybrid EEG-based control approach. Due to individual differences in EEG signals, the ERD/ERS pattern was used to identify whether the user is in the state of right-hand MI or non-right-hand MI.

In the CNN-LSTM model training process, each subject's data were used to train their own model. All data were divided into five parts randomly: three parts for the training set used for model construction (60% of the data), one part for the validation set used for optimal parameter selection (20% of the data), and one part for the testing set used for model evaluation (20% of the data). In addition, to compare with other methods, we selected three methods, i.e., CNN [43], LSTM [22], and CSP+SVM [44], to train the CNN-LSTM model on the same training set and then test these models using the same testing set.

B. ONLINE CONTROL EXPERIMENT

The aim of the online control experiment was to evaluate the performance of hybrid EEG-based control approach and the exosuit, as shown in Fig. 8. Subjects were asked to sit in a relaxed posture on a chair, facing a computer screen, while wearing the EEG cap and the exosuit. The subject's task was to complete the rehabilitation training pre-set by

FIGURE 8. Online control experimental scenario.

us, which was reminded in the form of speech. During the experiment, one of the seven movements would randomly appear, with each movement appearing nine times. Each subject needed to complete a total of 63 movements. After completing every three movements, there was a 10-second rest interval. For the three multi-joint movements, different joints are actuated in distinct sequences. In the drinking water movement, the sequence starts with the fingers, followed by the wrist, with the elbow and shoulder moving simultaneously. In the moving a cup movement, the fingers are actuated first, followed by the simultaneous movement of the wrist and shoulder. In the dumbbell lifting movement, the fingers are actuated first, followed by the wrist, and finally the elbow.

The flashing stimuli program guided subjects in the experiment. Firstly, it verbally announced a movement, and then the subjects selected the corresponding movement from 7 images. Once the selection was made by STEP1, the subjects performed right-hand MI, and the collected EEG signals were classified by the CNN-LSTM model. If the classification result was right-hand MI, the control signal was be transmitted to the actuation module.

C. USABILITY AND REHABILITATION ASSESSMENTS
1) USABILITY ASSESSMENT
Twelve participants (nine healthy graduate students and three moderate stroke survivors) took part in our usability assessment. They were invited to assess the ease of use and their user experience after using the exosuit we developed. We prepared a SUS questionnaire, comprising 5 positive statements and 5 negative statements. To better tailor the original SUS to our work, we have replaced "system" with "exosuit" from the original work, and adjusted the themes of Q7 and Q8 to "convenience" and "comfort". Each statement has a five-point scale, ranging from strongly disagree to strongly agree [50]. Odd-numbered questions Q1, Q3, Q5, Q7, and Q9 are positive, while the rest are negative. For odd-numbered questions, the score is the scale position minus 1. For even-numbered questions, the score is 5 minus the scale position. Multiply the sum of the scores by 2.5 to obtain the overall value of SUS. The SUS score ranges from 0 to 100.

2) REHABILITATION ASSESSMENT
To verify the multi-joint rehabilitative effectiveness of the exosuit, four stroke survivors with muscle weakness participated in our rehabilitation. They underwent a total of 35 days of rehabilitation training using our exosuit under guidance. In order to reduce participant fatigue and minimize the interference of data collection procedures with the rehabilitation process, and considering that we are capturing long-term trends, data were recorded every other day, totaling 18 days of data. Throughout the rehabilitation training, the subjects did not receive any other rehabilitation treatments. Each day of rehabilitation training, excluding preparation time, lasted approximately 15 minutes. The training included flexion movements of four joints involving muscles such as the pectoralis major, biceps brachii, flexor digitorum superficialis, and flexor carpi ulnaris muscle. If data collection was needed for the day, EMG sensors were attached to the aforementioned muscles during the flexion process to record EMG signals. Following the rehabilitation training, approximately 10 minutes of joint ROM recording (about 2.5 minutes per joint) was conducted. We use goniometers of various specifications to measure the ROM.

With the participants' consent, we used marking ink to label the electrode positions on the skin surface. This ink is harmless to the human body and can last for several days. Once the markings disappeared, they were reapplied to the original positions to ensure consistency of sensor placement.

IV. RESULTS AND DISCUSSIONS
A. CNN-LSTM PUBLIC DATASET RESULTS
To verify the effectiveness of our CNN-LSTM model, we firstly applied it to a public dataset. The dataset we used is the BCI Competition IV 2a dataset, where 9 subjects performed MI tasks of left hand, right hand, both feet, and tongue, with two sessions on different days recorded for each subject. Each session consisted of 6 runs, each comprising 48 trials (12 for each of the four possible classes), with short breaks between runs, yielding a total of 288 trials per session. For all 9 subjects, the average classification accuracy of CNN-LSTM model was 80.11%. Table 1 shows the comparison with other algorithms, which is a relatively good result. Our model demonstrated a certain advantage in terms of accuracy, and we believe that the CNN-LSTM cascaded model can indeed perform better in processing data with features such as time series and spatial information. However, to evaluate the effectiveness of the exosuit in practical use, online experiments are needed. Before that, our proposed hybrid EEG-based control approach requires offline training experiments to collect the EEG data of each subject and establish their own model.

B. RESULTS OF OFFLINE EXPERIMENT
1) ERD/ERS ANALYSIS
Fig. 9 shows the time course of ERD/ERS and EEG topographies. For left-hand and right-hand MI, the EEG power in
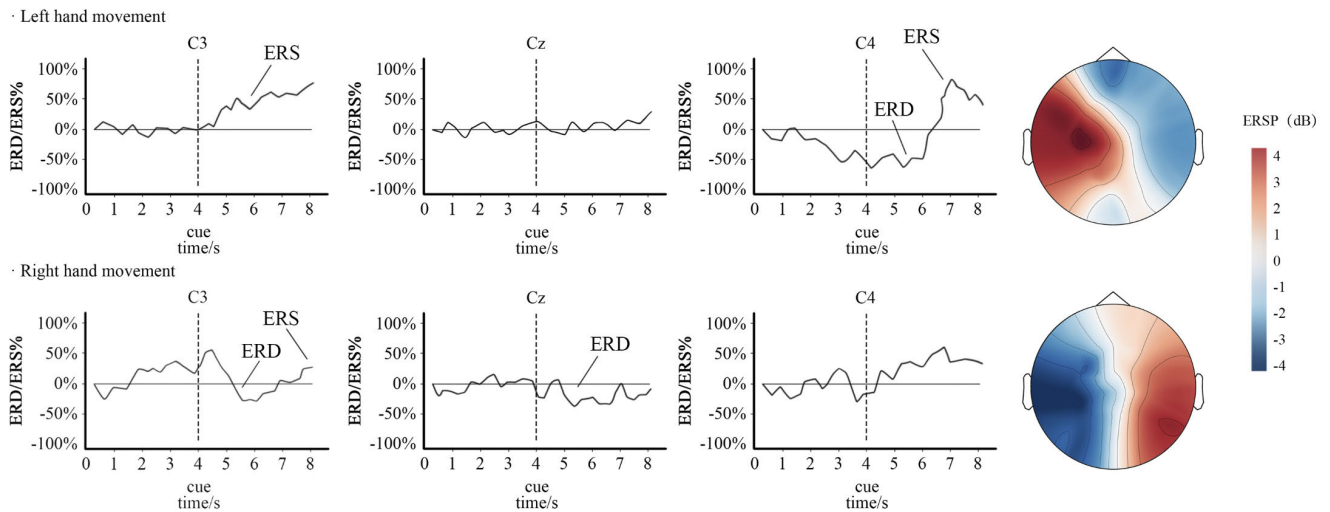
FIGURE 9. The time course of ERD/ERS from second 0 to 8 and EEG topographies from second 5 to 7 for left-hand and right-hand MI across all trials and all subjects.

**TABLE 1.** Accuracies of CNN-LSTM and other methods on BCI Competition IV Dataset 2a.

Methods	Subject									Avg.
	A01	A02	A03	A04	A05	A06	A07	A08	A09	
Gouy-Pailler et al. [45]	0.66	0.42	0.77	0.51	0.50	0.21	0.30	0.69	0.46	0.50
Ang et al. [46]	0.68	0.42	0.75	0.48	0.40	0.27	0.77	0.75	0.61	0.57
LDA	0.76	0.41	0.83	0.56	0.35	0.26	0.79	0.80	0.72	0.61
Vidaurre et al. [47]	0.76	0.38	0.87	0.60	0.46	0.34	0.77	0.76	0.74	0.63
Ai et al. [48]	0.77	0.54	0.84	0.70	0.63	0.61	0.77	0.84	0.86	0.73
Sakhavi et al. [33]	0.88	0.65	0.90	0.67	0.63	0.45	0.90	0.83	0.80	0.74
Fang et al. [49]	0.86	0.65	0.90	0.64	0.76	0.52	0.91	0.89	0.87	0.78
CNN-LSTM	0.89	0.62	0.91	0.73	0.79	0.66	0.91	0.85	0.85	0.80

the 8-12 Hz frequency band at C3, Cz, and C4 was averaged across all trials and subjects and displayed as relative percentage of EEG power compared to a reference period.

For left-hand MI, a significant ERD (5-7s) followed by an ERS (7-8s) was observed over the contralateral side C4. Meanwhile, a weaker ERS (5-7s) was observed over the ipsilateral side C3. For right-hand MI, an ERD and a weaker ERS were observed over the contralateral side C3, with a weaker ERD observed at Cz. EEG topographies of ERD/ERS patterns were further analyzed from 5 to 7 seconds for all trials and subjects, where blue indicates ERD (power decrease) and red indicates ERS (power increase).

2) MODEL CLASSIFICATION RESULTS

Table 3 presents the MI classification accuracies of the CNN-LSTM model for 8 subjects. We also established models using CNN, LSTM, and CSP+SVM for each subject for comparison with our CNN-LSTM model. The average classification accuracy of CNN-LSTM model (90.07% ± 2.23%) was 4.14%, 7.56%, and 10.06% higher than that of CNN (85.93% ± 2.14%), LSTM (82.51% ± 1.16%), and CSP+SVM (80.01% ± 1.92%), indicating better MI
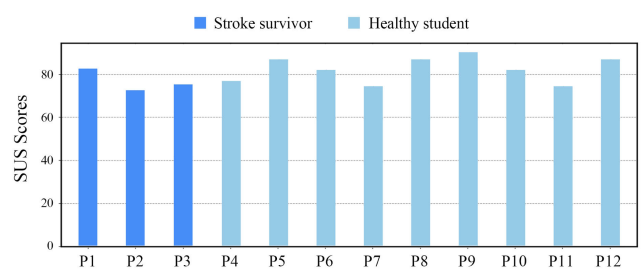
FIGURE 10. SUS scores of three stroke survivors and nine healthy students.

classification performance of the CNN-LSTM model. A 4 (CNN-LSTM, CNN, LSTM, and CSP+SVM) × 2 (left hand MI and right hand MI) repeated measures ANOVA was applied to evaluate the interaction of recognition method × MI class and the main effect of recognition method and MI class on the classification performance. A confidence level of 95% was selected. As show in Table 2, the results of variance analysis indicated no significant interaction effect between recognition method and MI class (F = 0.002, p > 0.05); recognition method had a significant effect on classification
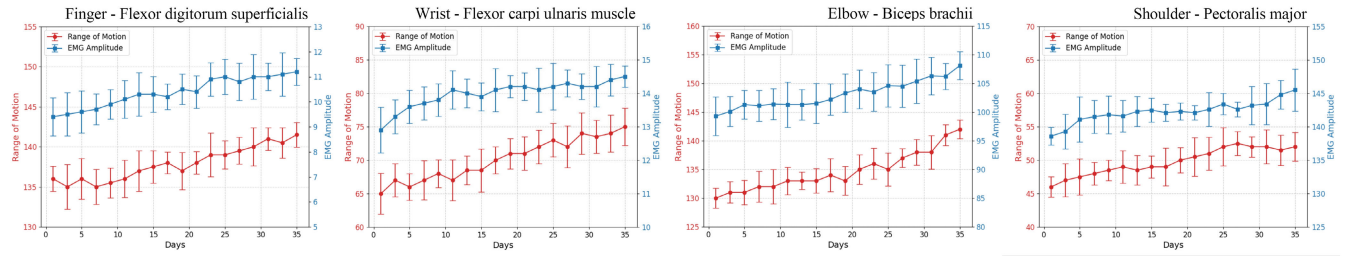
FIGURE 11. Records of range of motion and average EMG amplitude during 35-day rehabilitation training across all subjects.

TABLE 2. ANOVA results for recognition methods and MI classes.

Comparison	F-value	p-value
Recognition Method × MI Class Interaction	0.002	>0.05
Recognition Method Main Effect	98.583	<0.05
MI Class Main Effect	0.003	>0.05

TABLE 3. Classification accuracies of four methods on the same testing set for each subject.

Subject	Acc (%)			
	CNN-LSTM	CNN	LSTM	CSP+SVM
1	86.64	86.61	84.12	78.80
2	90.14	85.02	83.46	83.04
3	87.43	86.11	82.61	83.68
4	88.93	84.61	81.75	79.10
5	91.28	88.70	81.02	79.23
6	89.29	82.81	84.20	81.16
7	87.79	88.48	83.31	83.90
8	92.87	85.57	80.63	80.12
9	93.17	90.12	82.06	78.48
10	89.92	84.16	83.53	81.26
11	89.45	85.62	81.40	82.17
12	93.88	83.30	82.04	78.80
Average±std	90.07±2.23	85.93±2.14	82.51±1.16	80.01±1.92

TABLE 4. SSVEP accuracies, MI accuracies, and overall success rate of hybrid EEG-based control approach.

Subject	Acc (%)		Task Success Rate
	SSVEP	MI	
1	96.83	87.30	84.53
2	95.24	85.71	81.63
3	93.65	87.30	81.76
4	96.83	88.89	86.07
5	93.65	90.48	84.73
6	96.83	88.89	86.07
7	95.24	92.06	87.68
8	93.65	90.48	84.73
9	98.41	87.30	85.91
10	96.83	90.48	87.61
11	95.24	92.06	87.68
12	93.65	90.48	84.73
Average±std	95.50±1.57	89.29±1.96	85.26±1.95

reached 81.25 ± 5.82 (Cronbach's $\alpha = 0.64$), indicating a favorable level of usability.

2) REHABILITATION ASSESSMENT

An increase in the average EMG amplitude indicates a stronger electrical signal generated during muscle contraction, predicting an increase in muscle strength and contraction ability. Therefore, the average EMG amplitude serves as one of our reference indicators for evaluating rehabilitation effectiveness. During the muscle rehabilitation process, ROM of the joints also increases correspondingly with the increase in muscle strength and flexibility. By regularly monitoring changes in participants' ROM, we can assess their muscle rehabilitation progress.

According on our tracking records, the average rehabilitation effectiveness of the subjects is shown in Fig. 11. The 4 joints involved in rehabilitation exhibited an average ROM increase of 10.33%. The average EMG amplitude of the 4 main muscles involved in the movement of these 4 joints increased by 11.35%. We observed a decline in user attention and motivation during the long-term rehabilitation process. Subjects had reported that they needed to concentrate in order to continue with the rehabilitation process. This led us to consider adding more engaging content to the rehabilitation process to help maintain subjects' motivation.

performance ($F = 98.583$, $p < 0.05$), while MI class had no statistically significant effect on classification performance ($F = 0.003$, $p > 0.05$).

C. RESULTS OF ONLINE CONTROL EXPERIMENT

The results of task success rates for each subject in the online control experiment are shown in Table 4. Task success rate is defined as the percentage of successful execution of the selected movement by the subject, meaning it was successfully recognized in both STEP 1 and STEP 2. The average success rate for individual rehabilitation task was 85.26%±1.95%.

D. RESULTS OF ASSESSMENTS

1) USABILITY ASSESSMENT

Fig. 10 shows the SUS scores for all participants. P1, P2 and P3 represent stroke survivors, while the rest of the participants are healthy students. The average score of all participants

V. CONCLUSION

In this paper, we developed a 4-DOF exosuit for upper-limb rehabilitation that aimed at restoring movement ability in individuals with movement disorders due to stroke. The exosuit features active control performance, four-degree-of-freedom, portability, and lightweight. This active control is realized through a hybrid EEG-based control approach, integrating the SSVEP and MI paradigms. The hybrid approach leverages MVMD-CCA for SSVEP EEG recognition and a CNN-LSTM model for MI EEG recognition, demonstrating high classification accuracy. Another important goal of the hybrid EEG-based control approach is to facilitate an active, repetitive, and moderately intense rehabilitation process. As mentioned in the introduction, leveraging neuroplastic principles to develop rehabilitation methods based on active-ness, repetition, and specificity holds significant potential, although relevant confirmatory research is still underway.

The SUS scores demonstrate the favorable usability of the exosuit, with the majority of participants able to immediately engage in rehabilitation training. We recorded users' EMG amplitude and joint ROM during the 35-day rehabilitation training. The data we recorded showed an increase in both the average EMG amplitude and the average ROM, implying improvements in muscle strength and flexibility. In the future, we aim to further enhance the lightweight and reliability of the exosuit, and extend the exosuit to additional joints. Additionally, our goal is to optimize the MI algorithm to improve classification performance and enable multiple command outputs through MI.

CONFLICTS OF INTEREST

The authors declare that they have no known competing financial interests or personal relationships that could have appeared to influence the work reported in this paper.

REFERENCES

[1] C. O. Johnson et al., "Global, regional, and national burden of stroke, 1990–2016: A systematic analysis for the global burden of disease study 2016," *Lancet Neurol.*, vol. 18, no. 5, pp. 439–458, 1990.

[2] J. Liu, Y. Ren, D. Xu, S. H. Kang, and L.-Q. Zhang, "EMG-based real-time linear-nonlinear cascade regression decoding of shoulder, elbow, and wrist movements in able-bodied persons and stroke survivors," *IEEE Trans. Biomed. Eng.*, vol. 67, no. 5, pp. 1272–1281, May 2020.

[3] J. D. Lee, L. M. Mooney, and E. J. Rouse, "Design and characterization of a quasi-passive pneumatic foot-ankle prosthesis," *IEEE Trans. Neural Syst. Rehabil. Eng.*, vol. 25, no. 7, pp. 823–831, Jul. 2017.

[4] D. Buongiorno, E. Sotgiu, D. Leonardis, S. Marcheschi, M. Solazzi, and A. Frisoli, "WRES: A novel 3 DoF wrist exoskeleton with tendon-driven differential transmission for neuro-rehabilitation and teleoperation," *IEEE Robot. Autom. Lett.*, vol. 3, no. 3, pp. 2152–2159, Jul. 2018.

[5] D. Chiaradia, M. Xiloyannis, C. W. Antuvan, A. Frisoli, and L. Masia, "Design and embedded control of a soft elbow exosuit," in *Proc. IEEE Int. Conf. Soft Robot. (RoboSoft)*, Apr. 2018, pp. 565–571.

[6] T. Bützer, O. Lambercy, J. Arata, and R. Gassert, "Fully wearable actuated soft exoskeleton for grasping assistance in everyday activities," *Soft Robot.*, vol. 8, no. 2, pp. 128–143, Apr. 2021.

[7] C. Nam et al., "An exoneuromusculoskeleton for self-help upper limb rehabilitation after stroke," *Soft Robot.*, vol. 9, no. 1, pp. 14–35, Feb. 2022.

[8] Q. Wu, X. Wang, B. Chen, and H. Wu, "Design and fuzzy sliding mode admittance control of a soft wearable exoskeleton for elbow rehabilitation," *IEEE Access*, vol. 6, pp. 60249–60263, 2018.

[9] C. J. Nycz, T. Bützer, O. Lambercy, J. Arata, G. S. Fischer, and R. Gassert, "Design and characterization of a lightweight and fully portable remote actuation system for use with a hand exoskeleton," *IEEE Robot. Autom. Lett.*, vol. 1, no. 2, pp. 976–983, Jul. 2016.

[10] N. Lotti et al., "Soft robotics to enhance upper limb endurance in individuals with multiple sclerosis," *Soft Robot.*, vol. 11, no. 2, pp. 338–346, Apr. 2024.

[11] D. Piovesan et al., "Improving healthcare access: A preliminary design of a low-cost arm rehabilitation device," *J. Med. Devices*, vol. 14, no. 1, Mar. 2020, Art. no. 011103.

[12] H. Almusawi and G. Husi, "Design and development of continuous passive motion (CPM) for fingers and wrist grounded-exoskeleton rehabilitation system," *Appl. Sci.*, vol. 11, no. 2, p. 815, Jan. 2021.

[13] Y. An and C. Park, "Effects of a deep learning-based smartphone application on shoulder abduction kinematics and brain activation in adhesive capsulitis: A randomized controlled trial," *J. Mech. Med. Biol.*, vol. 21, no. 10, Dec. 2021, Art. no. 2140076.

[14] Z. Qi, W. Chen, J. Wang, J. Zhang, and X. Wang, "Lower limb rehabilitation exoskeleton control based on SSVEP-BCI," in *Proc. IEEE 16th Conf. Ind. Electron. Appl. (ICIEA)*, Chengdu, China, Aug. 2021, pp. 1954–1959.

[15] Y. Ren, Y.-N. Wu, C.-Y. Yang, T. Xu, R. L. Harvey, and L.-Q. Zhang, "Developing a wearable ankle rehabilitation robotic device for in-bed acute stroke rehabilitation," *IEEE Trans. Neural Syst. Rehabil. Eng.*, vol. 25, no. 6, pp. 589–596, Jun. 2017.

[16] N. Singh, M. Saini, N. Kumar, M. V. P. Srivastava, and A. Mehndiratta, "Evidence of neuroplasticity with robotic hand exoskeleton for post-stroke rehabilitation: A randomized controlled trial," *J. Neuroeng. Rehabil.*, vol. 18, no. 1, p. 76, May 2021.

[17] J. A. Kleim and T. A. Jones, "Principles of experience-dependent neural plasticity: Implications for rehabilitation after brain damage," *J. Speech, Language, Hearing Res.*, vol. 51, no. 1, p. 225, Feb. 2008.

[18] X. Huang, F. Naghdy, H. Du, G. Naghdy, and G. Murray, "Design of adaptive control and virtual reality-based fine hand motion rehabilitation system and its effects in subacute stroke patients," *Comput. Methods Biomech. Biomed. Eng., Imag. Visualizat.*, vol. 6, pp. 1–9, Jul. 2017.

[19] T. Proietti et al., "Combining soft robotics and telerehabilitation for improving motor function after stroke," *Wearable Technol.*, vol. 5, p. e1, Jan. 2024.

[20] J. R. Wolpaw, "Brain-computer interfaces (BCIs) for communication and control," in *Proc. 9th Int. ACM SIGACCESS Conf. Comput. Accessibility*, Tempe, AZ, USA. New York, NY, USA: ACM Press, Oct. 2007, pp. 1–2.

[21] E. Yin, Z. Zhou, J. Jiang, F. Chen, Y. Liu, and D. Hu, "A speedy hybrid BCI spelling approach combining P300 and SSVEP," *IEEE Trans. Biomed. Eng.*, vol. 61, no. 2, pp. 473–483, Feb. 2014.

[22] J. Zhou, M. Meng, Y. Gao, Y. Ma, and Q. Zhang, "Classification of motor imagery EEG using wavelet envelope analysis and LSTM networks," in *Proc. Chin. Control Decis. Conf. (CCDC)*, Shenyang, China, Jun. 2018, pp. 5600–5605.

[23] E. Yin, Z. Zhou, J. Jiang, F. Chen, Y. Liu, and D. Hu, "A novel hybrid BCI speller based on the incorporation of SSVEP into the P300 paradigm," *J. Neural Eng.*, vol. 10, no. 2, Apr. 2013, Art. no. 026012.

[24] Y. Wang, X. Gao, B. Hong, C. Jia, and S. Gao, "Brain-computer interfaces based on visual evoked potentials," *IEEE Eng. Med. Biol. Mag.*, vol. 27, no. 5, pp. 64–71, Sep. 2008.

[25] X. Gao, D. Xu, M. Cheng, and S. Gao, "A BCI-based environmental controller for the motion-disabled," *IEEE Trans. Neural Syst. Rehabil. Eng.*, vol. 11, no. 2, pp. 137–140, Jun. 2003.

[26] H. Bakardjian, T. Tanaka, and A. Cichocki, "Optimization of SSVEP brain responses with application to eight-command brain–computer interface," *Neurosci. Lett.*, vol. 469, no. 1, pp. 34–38, Jan. 2010.

[27] K. Wang, D.-H. Zhai, Y. Xiong, L. Hu, and Y. Xia, "An MVMD-CCA recognition algorithm in SSVEP-based BCI and its application in robot control," *IEEE Trans. Neural Netw. Learn. Syst.*, vol. 33, no. 5, pp. 2159–2167, May 2022.

[28] L. Cheng, R. Wang, and Y. Zhang, "Decoding SSVEP patterns from EEG via multivariate variational mode decomposition-informed canonical correlation analysis," *Biomed. Signal Process. Control*, vol. 71, Jan. 2022, Art. no. 103209.

[29] S. Chaudhary, S. Taran, V. Bajaj, and A. Sengur, "Convolutional neural network based approach towards motor imagery tasks EEG signals classification," *IEEE Sensors J.*, vol. 19, no. 12, pp. 4494–4500, Jun. 2019.

[30] G. Pfurtscheller, C. Neuper, D. Flotzinger, and M. Pregenzer, "EEG-based discrimination between imagination of right and left hand movement," *Electroencephalogr. Clin. Neurophysiol.*, vol. 103, no. 6, pp. 642–651, Dec. 1997.

[31] L. Hu, J. Xie, C. Pan, X. Wu, and D. Hu, "Multi-feature fusion method based on WOSF and MSE for four-class MI EEG identification," *Biomed. Signal Process. Control*, vol. 69, Aug. 2021, Art. no. 102907.

[32] Y. R. Tabar and U. Halici, "A novel deep learning approach for classification of EEG motor imagery signals," *J. Neural Eng.*, vol. 14, no. 1, Feb. 2017, Art. no. 016003.

[33] S. Sakhavi, C. Guan, and S. Yan, "Learning temporal information for brain-computer interface using convolutional neural networks," *IEEE Trans. Neural Netw. Learn. Syst.*, vol. 29, no. 11, pp. 5619–5629, Nov. 2018.

[34] S. Pattnaik, M. Dash, and S. K. Sabut, "DWT-based feature extraction and classification for motor imaginary EEG signals," in *Proc. Int. Conf. Syst. Med. Biol. (ICSMB)*, Kharagpur, India, Jan. 2016, pp. 186–201.

[35] R. Zhang, Q. Zong, L. Dou, and X. Zhao, "A novel hybrid deep learning scheme for four-class motor imagery classification," *J. Neural Eng.*, vol. 16, no. 6, Oct. 2019, Art. no. 066004.

[36] R. T. Schirrmeister et al., "Deep learning with convolutional neural networks for EEG decoding and visualization: Convolutional neural networks in EEG analysis," *Hum. Brain Mapping*, vol. 38, pp. 5391–5420, Nov. 2017.

[37] P. Wang, A. Jiang, X. Liu, J. Shang, and L. Zhang, "LSTM-based EEG classification in motor imagery tasks," *IEEE Trans. Neural Syst. Rehabil. Eng.*, vol. 26, no. 11, pp. 2086–2095, Nov. 2018.

[38] A. Guzik-Kopyto, R. Michnik, P. Wodarski, and I. Chuchnowska, "Determination of loads in the joints of the upper limb during activities of daily living," in *Advances in Intelligent Systems and Computing*, vol. 472. Cham, Switzerland: Springer, 2016, pp. 99–108.

[39] I. Gaponov, D. Popov, S. J. Lee, and J.-H. Ryu, "Auxilio: A portable cable-driven exosuit for upper extremity assistance," *Int. J. Control, Autom. Syst.*, vol. 15, no. 1, pp. 73–84, Feb. 2017.

[40] E. Yin, Z. Zhou, J. Jiang, Y. Yu, and D. Hu, "A dynamically optimized SSVEP brain–computer interface (BCI) speller," *IEEE Trans. Biomed. Eng.*, vol. 62, no. 6, pp. 1447–1456, Jun. 2015.

[41] J. Jin, Z. Wang, R. Xu, C. Liu, X. Wang, and A. Cichocki, "Robust similarity measurement based on a novel time filter for SSVEPs detection," *IEEE Trans. Neural Netw. Learn. Syst.*, vol. 34, no. 8, pp. 4096–4105, Aug. 2021.

[42] N. ur. Rehman and H. Aftab, "Multivariate variational mode decomposition," *IEEE Trans. Signal Process.*, vol. 67, no. 23, pp. 6039–6052, Dec. 2019.

[43] N. Shajil, S. Mohan, P. Srinivasan, J. Arivudaiyanambi, and A. A. Murrugesan, "Multiclass classification of spatially filtered motor imagery EEG signals using convolutional neural network for BCI based applications," *J. Med. Biol. Eng.*, vol. 40, no. 5, pp. 663–672, Oct. 2020.

[44] H. Sun, Y. Xiang, Y. Sun, H. Zhu, and J. Zeng, "On-line EEG classification for brain-computer interface based on CSP and SVM," in *Proc. 3rd Int. Congr. Image Signal Process.*, vol. 9, Yantai, China, Oct. 2010, pp. 4105–4108.

[45] C. Gouy-Pailler, M. Congedo, C. Brunner, C. Jutten, and G. Pfurtscheller, "Nonstationary brain source separation for multiclass motor imagery," *IEEE Trans. Biomed. Eng.*, vol. 57, no. 2, pp. 469–478, Feb. 2010.

[46] K. K. Ang, Z. Y. Chin, C. Wang, C. Guan, and H. Zhang, "Filter bank common spatial pattern algorithm on BCI competition IV datasets 2a and 2b," *Frontiers Neurosci.*, vol. 6, p. 39, Mar. 2012.

[47] C. Vidaurre, M. Kawanabe, P. von Bünau, B. Blankertz, and K. R. Müller, "Toward unsupervised adaptation of LDA for brain–computer interfaces," *IEEE Trans. Biomed. Eng.*, vol. 58, no. 3, pp. 587–597, Mar. 2011.

[48] Q. Ai et al., "Feature extraction of four-class motor imagery EEG signals based on functional brain network," *J. Neural Eng.*, vol. 16, p. 026032, Apr. 2019.

[49] H. Fang, J. Jin, I. Daly, and X. Wang, "Feature extraction method based on filter banks and Riemannian tangent space in motor-imagery BCI," *IEEE J. Biomed. Health Informat.*, vol. 26, no. 6, pp. 2504–2514, Jun. 2022.

[50] J. Brooke et al., "SUS—A quick and dirty usability scale," *Usability Eval. Ind.*, vol. 189, no. 194, pp. 4–7, 1996.

• • •